Sequential ion-ion reactions for enhanced gas-phase sequencing of large intact proteins in a tribrid Orbitrap mass spectrometer

Jake T. Kline,[1] Christopher Mullen,[2] Kenneth R. Durbin,[3] Ryan N. Oates,[1] Romain Huguet,[2] John E. P. Syka,[2] Luca Fornelli[1,*]

[1] *Department of Biology, University of Oklahoma, 730 Van Vleet oval, Norman, Oklahoma 73019, United States*

[2] *Thermo Fisher Scientific, 355 River Oaks Parkway, San Jose, California 95134, United States*

[3] *Proteinaceous, Inc., Evanston, Illinois 60208, United States*

* To whom correspondence should be addressed: Department of Biology, University of Oklahoma, 730 Van Vleet oval, Richards Hall 417, Norman, Oklahoma 73019; e-mail: luca.fornelli@ou.edu; phone: 405-325-1483; fax: 405-325-6202.

Abstract

Obtaining extensive sequencing of an intact protein is essential in order to simultaneously determine both the nature and exact localization of chemical and genetic modifications which distinguish different proteoforms arising from the same gene. To effectively achieve such characterization is necessary to take advantage of the analytical potential offered by the top-down mass spectrometry (TDMS) approach to protein sequence analysis. However, as a protein increases in size, its gas-phase dissociation produces overlapping, low signal-to-noise fragments. The application of advanced ion dissociation techniques such as electron transfer dissociation (ETD) and ultraviolet photodissociation (UVPD) can improve the sequencing results compared to slow-heating techniques such as collisional dissociation; nonetheless, even ETD and UVPD-based approaches have thus far fallen short in their capacity to reliably enable comprehensive characterization of proteoforms ≥30 kDa. To overcome this issue, we have applied proton transfer charge reduction (PTCR) to limit signal overlap in tandem mass spectra (MS^2) produced by ETD (alone or with supplemental ion activation, EThcD). Compared to conventional MS^2 experiments, following ETD/EThcD MS^2 with PTCR MS^3 prior to m/z analysis of deprotonated product ions in the Orbitrap mass analyzer proved beneficial for the identification of additional large protein fragments (≥10 kDa), thus improving the overall sequencing and in particular the coverage of the central portion of all four analyzed proteins spanning from 29 to 56 kDa. Specifically, PTCR-based data acquisition led to 39% sequence coverage for the 56 kDa glutamate dehydrogenase, further increased to 44% by combining fragments obtained via HCD followed by PTCR MS^3.

Introduction

The main allure of top-down mass spectrometry (TDMS)[1] is its potential to enable full characterization of different proteoforms[2] derived from the same gene but carrying different patterns of post-translational modifications (PTMs) and genetic modifications (e.g., single nucleotide polymorphisms leading to amino acid substitution). Improving sequence coverage obtained through gas-phase dissociation and mass-over-charge (m/z) analysis of proteoform ions increases the accuracy of identification of modification sites; therefore, sequence coverage is the primary metric for measuring success in proteoform characterization. Typically, the difficulty of this endeavor is inversely proportional to the mass of the proteoform being analyzed. For small proteins such as ubiquitin or histones, achieving high levels of sequence coverage is relatively straightforward.[3-4] At present, the major hurdle for TDMS is the efficient amino acid sequencing of larger proteoforms, typically ≥ 30 kDa.

Two main challenges can be readily identified in the gas-phase sequencing of proteoforms composed of hundreds of amino acid residues. First, the polypeptide backbone should be cleaved at as many positions as possible; secondly, the generated fragments should be present as well-resolved isotopic clusters to facilitate deconvolution and interpretation of product ion mass spectra, ideally leading to the identification of both fragments derived from a single backbone cleavage to improve the confidence in cleavage assignment. The former challenge can be addressed through the application of advanced ion dissociation techniques.[5] Several studies have provided convincing evidence that, while vibrational energy threshold methods are highly efficient – with efficiency of fragmentation defined as the ratio between the ion current of product ions

to that of the selected precursor –, ion dissociation techniques based on the interaction of protein cations with electrons[6] or high-energy photons[7] produce more extensive and randomized fragmentation, particularly for larger proteins. Radical driven methods, specifically electron capture dissociation (ECD)[8] and electron transfer dissociation (ETD),[9] have been applied since their invention to the analysis of intact proteins. ECD implementation had been long limited to Fourier transform–ion cyclotron resonance mass spectrometers (FT-ICR),[10] where it was successfully applied to the characterization of intact proteins up to ~150 kDa.[11-12] Recently, ECD has been successfully applied to other types of instrument platforms equipped with time-of-flight (TOF)[13] or Orbitrap mass analyzers.[14] Conversely, since its inception ETD has equipped different instruments with hybrid designs thanks to its less demanding working conditions (i.e., higher pressure regime) that make it compatible with radio frequency (RF) ion trap devices.[15-16] Examples of ETD-based characterization of whole proteins ≥30 kDa include the use of high-resolution quadrupole-TOF instruments[17-18] as well as hybrid linear ion trap (LTQ)-Orbitrap[19] and tribrid quadrupole- Orbitrap-LTQ[20] instruments. While ETD alone can lead to high sequence coverage (up to ~35%) for proteins as large as an intact 150 kDa immunoglobulin G,[19-21] even more extensive sequencing can be obtained when disrupting non-covalent interactions that prevent the separation of already dissociated protein fragments (typically leading to the observation of intact charge-reduced precursor species, ETnoD products) by supplying either the totality of ETD products or the undissociated precursor with additional vibrational energy. Originally developed for enhancing the quality of ECD spectra through the irradiation of ECD-generated charge-reduced species with low-energy infrared photons in experiments termed activated-ion ECD (AI-ECD),[22] this same concept is implemented in ETD-enabled mass spectrometers in a variety of ways.[23-24] Specifically, the odd-electron precursor cations can be further

activated using low-energy collision-induced dissociation (CID) in the ion trap in experiments termed ETciD;[25] or all the ETD products can be transferred to a collision cell to be subjected to re-activation through beam-type higher-energy collisional dissociation (HCD),[26] applying a supplemental activation strategy named EThcD.[27] In another approach, cations can be irradiated with 10 μm photons generated by a CO_2 laser during the ETD reaction, in experiments typically referred to as AI-ETD.[28-30] In their application to TD MS, EThcD and AI-ETD have proven superior to ETD in generating a larger number of *c*- and *z*-type ions along with *b*- and *y*-types, ultimately increasing sequence coverage of larger proteins. For example, Riley *et al.* reported up to 25% coverage of the 66 kDa bovine serum albumin performing AI-ETD tandem mass spectrometry (MS^2) on a tribrid Orbitrap instrument, whereas ETD MS^2 produced 19% coverage.[31]

Alternatively, ultraviolet photodissociation (UVPD) performed using 193 or 213 nm photons has also proven effective in the fragmentation of large protein cations, offering the possibility of randomly cleaving the backbone at any of its three covalent bonds (C_α-C, C-N, N-C_α) thus generating up to 9 different odd- or even-electron ion types (without counting side chain losses).[32-33] Direct comparisons between UVPD and other techniques such as ETD or HCD have shown that the use of high-energy photons can produce highly dense MS^2 spectra and outperform rival techniques in term of sequence coverage and number of identified unique backbone cleavages.[32, 34] Like ETD, UVPD is particularly effective if spectral averaging (or averaging of time-domain transients in Fourier transform mass spectrometry, FTMS) is applied to improve signal-to-noise ratio (S/N), as UVPD is generally not as efficient as HCD and ion current is diluted into multiple fragmentation channels. Furthermore, UVPD was demonstrated to be

complementary to ETD and HCD in terms of amino acid cleavage propensities and portions of a protein's sequence preferentially fragmented.[33]

Nonetheless, even considering the impressive improvements in whole protein characterization offered by the most advanced ion dissociation techniques, the second challenge related to the detection of product ions and subsequent interpretation of resulting MS^2 spectra – spectral congestion – remains. In the case of large proteoforms, the dilution of the precursor ion current into a myriad of fragmentation channels can lead to lower abundances and poor ion statistics for fragment ions, not only reducing their S/N but can also negatively affecting the relative isotopic abundances within single ion isotopic clusters. In the common case of experiments conducted using electrospray under denaturing conditions, the high protonation of the resulting precursors further exacerbates these issues,[35] as each backbone cleavage typically results in the formation of a distribution of charge states for the product ions, likely reflecting the fact that multiple "protonation isomers" are present for each proteoform cation. As a result, low abundant, multiply charged product ions often overlap in the m/z space, rendering their identification difficult or even impossible. Additionally, sequence uninformative species such as leftover precursor (in ETD/ECD and derivate techniques, and also in UVPD) and charge-reduced species (ETD/ECD) are often highly abundant and hinder the clear detection of other ion species in close m/z proximity. This is also a known issue in UVPD MS^2 spectra where distribution of m/z values for the larger mass product ions are primarily centered around the intact precursor m/z.[7]

Gas-phase fractionation (GPF) is an approach that has been utilized to improve detection of proteoforms[36] and also to enhance the performance of imaging mass spectrometry;[37] therefore, its application could also be beneficial for improving the

quality of MS^2 spectra of whole proteoforms. However, GPF could increase spectral dynamic range but would not solve the signal interference problem. For this reason, non-dissociative ion-ion reactions in the gas-phase,[38-39] and specifically proton transfer reactions,[40-41] are currently finding application[42] in the field of TDMS though having being first described in the nineties. In ion-ion proton transfer reactions, multiply charged cations are reacted with anions (typically singly charged perfluorinated species)[43] to form a deprotonated cations – which will be subsequently detected at a higher m/z values – and a neutral molecule (the original anion) that cannot interfere with the m/z analysis. The application of proton transfer reactions in TDMS MS^3 strategies (where precursor fragmentation is followed by deprotonation of product ions prior to high resolution m/z detection) has proven beneficial for decongestion of MS^2 spectra of intact proteins resulting from either ETD[44] or UVPD events,[45-46] allowing the detection and sequence-matching of fragments otherwise unidentified in canonical MS^2 experiments.

In this study, we describe the combination of electron-based dissociation techniques (ETD, and EThcD) with the commercial implementation of ion-ion proton transfer reactions termed proton transfer charge reduction (PTCR),[47] available in the latest generation of tribrid Orbitrap mass spectrometers, the Orbitrap Eclipse. We demonstrate the improvements in protein sequencing obtained over standard MS^2 experiments when performing PTCR MS^3 experiments with different degrees of complexity. Additionally, we apply the PTCR MS^3 strategy to a non-electron based dissociation method, HCD, which is commonly utilized in TDMS and is complementary to ETD, as a further point of comparison to evaluate the utility of the PTCR MS^3 TDMS methods for analysis of proteins of molecular weight above 30 kDa.

Experimental Section

Materials. Bovine carbonic anhydrase II (catalog number C2624), rabbit aldolase (catalog number A2714), *Saccharomyces cerevisiae* enolase (catalog number E6126), and bovine liver glutamate dehydrogenase (catalog number G7882) were purchased from Millipore Sigma (St. Louis, MO). Lyophilized protein stocks were resuspended in water to a concentration of 2 mg/mL then desalted using Pierce Zeba spin columns (Thermo Scientific, Rockford IL) following the manufacturer's suggested protocol. Proteins were diluted to 1 μM in 50%/50% acetonitrile/water (v:v) with 0.1% formic acid. All solvents were obtained in LC-MS purity grade from Fisher Scientific (Houston, TX).

Mass Spectrometry. All experiments were performed on an Orbitrap Eclipse mass spectrometer (Thermo Scientific, San Jose, CA) equipped with a front-end auxiliary ionization source[48] with a dual inlet for ETD and PTCR reagents (i.e., Easy-ETD and PTCR options). Protein solutions were directly infused at 0.7-1 μL/min and ionized using a custom-made nano-electrospray source to which a 1.7-2.0 kV potential was applied. The mass spectrometer was operated in intact protein mode at 3 mTorr of N_2 pressure in the ion-routing multipole. The heated capillary was set at 320˚ C, and an offset of 15 V between SRIG and MP00 was applied to favor ion declustering and desolvation. Source RF was set at 30%. MS^1 spectra were collected in the orbitrap mass analyzer at 7,500 resolution (at *m/z* 200) while averaging five transients (i.e., microscans) per spectrum. For MS^2 and MS^3 experiments, the automatic gain control (AGC) target for each precursor was set at 2000% (corresponding to 1e6 charges), and spectra were recorded at 240,000 resolution (at *m/z* 200) averaging ten microscans/spectrum in "full profile" mode (i.e., without automatic noise thresholding). MS^2 experiments were recorded over a 400-2000 *m/z* window, while MS^3 experiments used an extended 500-8000 *m/z*

window (available through the HMR^n option). Protein precursors were *m/z* selected with the quadrupole *m/z* filter (isolation width: 2 *m/z* units) and dissociation was performed via HCD, ETD and EThcD. HCD experiments utilized 29-33% normalized collision energy (NCE) applying precursor charge state correction for optimized setting of collision energy. ETD was performed for 2-7 ms (fluoranthene reagent ion target: 1.5e6 charges). EThcD experiments where performed by following ETD with HCD activation of all reaction products using 15% NCE. PTCR MS^3 experiments were performed as previously described[47] with a target value for the reagent (perfluoroperhydrophenanthrene anions, PFPP, mass = 624 Da, Sigma Selectophore 56919) of 2e6 charges for single MS^3 isolation window experiments, and 1e6 charges for multiwindow experiments. Two main sets of PTCR MS^3 experiments were designed, as shown in **Figure 1**: in the first set, the whole product ion population generated by HCD, ETD or EThcD MS^2 was isolated in the high pressure cell of the dual cell linear ion trap using a wide isolation window (width: 1800 *m/z* units, including all products between 200 and 2000 *m/z*), and all MS^2 products were subjected to PTCR simultaneously. Hereinafter, these experiments will be indicated as "1x1800 PTCR MS^3". For the second set, MS^2 fragmentation products were divided into six sub-populations based on their *m/z* position, and each of these was isolated in the LTQ and subjected to PTCR one at a time. These experiments will be indicated as "6x250 PTCR MS^3" throughout the rest of the manuscript. PTCR duration was varied depending on the complexity of the product ion population, with experiments using a single isolation window using longer reaction times (20-50 ms) than those based on a narrow isolation window (2-20 ms). Further details for the 6x250 PTCR MS^3 experiments are reported in **Table S1**. All measurements were performed in triplicate. A complete list of all the different conditions tested for the 4 standard proteins and their respective

efficacy (measured as resulting sequence coverage and number of matched unique product ions) is provided in **Figures S1-S4** (Supporting Information).

Data analysis. For each experiment, MS^2 or MS^3 spectra were averaged in Qual Browser (Thermo Scientific) and exported as a single spectrum RAW file. For carbonic anhydrase II, fifteen spectra were averaged (for a total of 150 transients) in both MS^2 and PTCR MS^3 experiments. For aldolase, enolase, and glutamate dehydrogenase in both MS^2 and PTCR MS^3 experiments, twenty spectra were averaged (for a total of 200 transients). Single spectrum RAW files were batch-loaded into TDValidator Pro (Proteinaceous Inc, Evanston, IL),[20] and matched against theoretical fragment ion isotopic distributions from protein sequences obtained from the UniProt knowledgebase (accession P00921 for carbonic anhydrase II, P00883 for aldolase, P00924 for enolase, and P00366 for glutamate dehydrogenase). A complete list of the parameters used for fragment matching is reported in **Table S2** while the rationale for the parameter selection is described in "Results and discussion". Graphical fragmentation maps were obtained directly in TDValidator in the case of MS^2 experiments and 1x1800 PTCR MS^3 experiments, while they maps for "narrow isolation" 6x250 PTCR MS^3 experiments were obtained by combining the lists of masses of matched fragments for each of the 6 isolation windows in ProSight Lite.[49-50] Final graphs including violin plots were generated using GraphPad Prism 9 (GraphPad Software, San Diego, CA).

Results and discussion.

Preliminary test runs (including both MS^2 and PTCR MS^3 experiments) were performed using all four proteins to determine appropriate fragment matching parameters to apply in TDValidator Pro to the analysis of hundreds of spectra (resulting from all the tested experimental conditions summarized in **Figures S1-S4**). Mass spectra resulting from

test runs were manually validated in TDValidator Pro starting from "loose" parameters – ion S/N cutoff 5, similarity score (which accounts for the relative abundances of the isotopomers in a cluster) 0.5, fragment mass tolerance 10 ppm, inter-isotopomer tolerance 3 ppm. After validation, various combinations of more stringent parameter sets were tested in order to automatically eliminate the vast majority of false positives while retaining the validated true positive matches. The final parameters for each experiment type are reported in **Table S2**, while examples of the comparison between the manually validated set of matched product ions and their automatically obtained counterparts (represented by Venn diagram) are displayed in **Figure S5**. Using the final parameter values for each experiment type, the overlap between the two fragment lists is of at least 80%, and the respective sequence coverages differ of less than 4%. Not surprisingly, the finalized set of parameters differ only minimally among ion dissociation techniques, while a larger variation in the optimal values is observed between MS^2 and PTCR MS^3 experiments, with the former data type requiring more stringent parameters than the latter. We attribute this discrepancy to the spectral congestion that characterizes MS^2 spectra, with highly charged product ion clusters overlapping with each other in the m/z vicinity of the precursor and any intact charge reduced products. Such signal interference is practically absent in PTCR MS^3 spectra, where the rare cases of signal overlap are typically solved thanks to the high resolving power offered by the Orbitrap mass analyzer in conjunction with the low charge state of PTCR-deprotonated fragment ions. The difference in spectral congestion between MS^2 and corresponding PTCR MS^3 experiments can be appreciated in **Figures S6-S7**, comparing 3 ms EThcD spectra resulting from the fragmentation of the 42+ charge state of aldolase with or without subsequent PTCR of product ions. Visually, the spectral density observed in 100 m/z-wide windows in the MS^2 spectrum is comparable to that of 1000 m/z-wide

windows in the PTCR MS^3 spectrum. Overall, we believe that applying data-driven decisions for data analysis ensured the reliability of the results discussed hereinafter.

We started our MS^2 vs PTCR MS^3 comparison with the 29 kDa carbonic anhydrase, commonly used as a standard in top-down MS and for which an extensive comparative literature exists. Using the Orbitrap Eclipse, ETD MS^2 spectra obtained by averaging 150 transients returned 70%, 75% and 64% sequence coverage for charge states 25+, 30+ and 35+, respectively (**Figure S8A**). When EThD was used, the coverage went up to 77% (**Figure 2A**). These results compare favorably with previous works which used electron-based ion activations on an Orbitrap Fusion Lumos: by averaging 300 microscans, Riley *et al.* reported nearly 70% sequence coverage on carbonic anhydrase fragmented with AI-ETD, while in the same study the coverage obtained via ETD and EThcD fell slightly short of 60% regardless of the selected precursor charge states. Almost 200 unique fragments were matched in our ETD experiments (searching uniquely for *c*- and *z*-type ions); EThcD experiments on the Orbitrap Eclipse returned ~250 matched unique product ions (including also *b*- and *y*-type ions), by that outperforming of ~15% the best AI-ETD results available in literature (**Figure 2B**). Despite an early report where 81% sequence coverage was shown on an Orbitrap Elite,[32] other studies based on 193 nm UVPD claim that the coverage of carbonic anhydrase reaches typically ~60-70% across different FTMS platforms.[46, 51] The most recent work based on an Orbitrap Fusion Lumos reported 63% sequence coverage for UVPD MS^2 of the 25+ precursor, with ~250 unique fragments matched (searching for 9 different product ion types).[45] These comparisons are important to evaluate the impact of the technical improvements introduced with the latest generation of tribrid Orbitrap mass spectrometers on top-down MS: we attribute the observed boost in MS^2 performance primarily to the redesigned high pressure cell of the dual cell linear ion trap which offers

better control of the ion-ion reaction kinetics via higher reagent capacity and, more importantly, to a significantly enhanced ion transmission from the LTQ to the C-trap and the Orbitrap owing to a redesigned ultra-high vacuum chamber. Despite the high bar set by MS^2 experiments, the 1x1800 PTCR MS^3 experiments using a single, wide isolation window completely outperformed the MS2 runs: for both ETD and EThcD an increase in the number of unique matched fragments was observed (**Figure S8B** and **Figure 2B**, respectively), and the sequence coverage also increased for all the precursors, reaching up to 90% coverage for the 35+ precursor using EThcD. Notably, EThcD MS^2 - 1x1800 PTCR MS^3 experiments slightly outperformed the corresponding ones by Sanders *et al.* based on 193 nm UVPD which produced ~80% sequence coverage. Finally, the 6x250 PTCR MS^3 experiments based on the fractionation of product ions to charge-reduce into 6 sub-populations produced a noticeable increase in the number of matched product ions. This increase also translated into an increase of sequence coverage for ETD, where the coverage consistently exceeded 80% across the three selected charge states with a maximum of 86% for the 35+ precursor. Conversely, EThcD reached up to 89% sequence coverage, essentially the same value reached via the 1x1800 PTCR MS^3 runs. A lack of improvement in sequence coverage despite an increase in the number of unique matched fragments was reported also by Sanders *et al.* for the corresponding UVPD-based experiments followed by proton transfer reaction that used 10 narrow isolation windows. Importantly, the violin plots for ETD and EThcD experiments (**Figure S8C** and **Figure 2C**, respectively) show that even for this relatively small protein PTCR MS^3 allows the identification of large product ions which would otherwise be undetected in MS^2 experiments, likely due to elevated spectral congestion. Stunningly, by passing from MS^2 to 6x250 PTCR MS^3 experiments the number of complementary ion pairs (e.g., N- and C-terminal containing product ions arising from

the same backbone cleavage) increased from 13 to 134 for ETD and from 12 to 118 for EThcD, respectively (**Figure S8D** and **E**, **Figure 2D** and **E**).

When the mass of the analyzed protein was increased, the differences between ETD/EThcD sequence coverage results obtained without or with charge reduction of product ions became more apparent. For 39 kDa aldolase, passing from MS^2 to 1x1800 PTCR MS^3 experiments resulted in an additional 10-15% sequence coverage (from 53% to 64% for ETD and from 55% to 70% for EThcD, **Figure S9A** and **Figure 3A**). The only exception was when ETD was performed on the 52+ precursor and no significant benefit was derived from PTCR. The 6x250 PTCR MS^3 experiments contributed an additional 12-14% sequence coverage, which led to 76% sequence coverage for ETD and 84% for EThcD. Importantly, the 6x250 PTCR MS^3 strategy doubled the number of unique matched fragments compared to the corresponding MS^2 experiments for both ETD and EThcD; fragmenting the 42+ precursor with EThcD, the 6x250 PTCR MS^3 runs returned a total of 480 unique fragments (**Figure S9B** and **Figure 3B**). As shown in **Figure S9C** and **Figure 3C**, the majority of the additional product ions identified via charge reduction have mass larger than 10 kDa, with the largest fragments identified having masses close to that of the precursor (i.e., ≥30 kDa). As shown in **Figure S9D** and **E** for ETD, and **Figure 3D** and **E** for EThcD, the MS^2 experiments failed to provide sequence coverage for the central portion of the protein (amino acid residues 150-200), whereas PTCR MS^3 strategies (and particularly the 6x250) led to the identification of a number of complementary product ions in that region. More precisely, the total number of complementary product ion pairs increased from 0 to 83 for ETD and from 6 to 81 for EThcD.

For 46 kDa enolase, following ETD or EThcD with PTCR produced a substantial increase in sequence coverage: ETD MS^2 resulted in over 40% sequencing (specifically, 41%, 44% and 45% for charge states 50+, 55+ and 60+, respectively), and EThcD MS^2 slightly exceeded these values, reaching 45% coverage for both the 55+ and 60+ precursors (**Figure S10A** and **Figure 4A**, respectively); the sequence coverage was substantially raised to 59% and 66% through the application of PTCR following ETD and EThcD, respectively. Differently from aldolase, no major difference in sequence coverage or in the count of unique identified fragments resulted from the use of the 6 narrower isolation windows in place of the single 1800 *m/z*-wide one for enolase (**Figure S10B** and **Figure 4B**). Interestingly, using EThcD the upper mass distribution of identified enolase fragments does not increase proportionally to the degree of experimental complexity: while in ETD we observe a substantial increase in the median of the fragment mass moving from MS^2 to 1x1800 PTCR MS^3 runs, and from there to 6x250 PTCR MS^3 experiments (**Figure S10C**), in the case of EThcD the highest median value is reached with the 1x1800 PTCR MS^3 experiments, for all the three analyzed precursor charge states (**Figure 4C**). As observed for aldolase, charge reduction via proton transfer facilitated the identification of complementary product ion pairs, not observed in MS^2 experiments where only the terminal portions of the protein were sequenced (**Figure S10D** and **Figure 4D**). Specifically, 8 complementary pairs were identified using ETD and 4 using EThcD in the 6x250 PTCR MS^3 runs (**Figure S10E** and **Figure 4E**, respectively). By applying PTCR, the longest portion of the protein that remain unsequenced is 14 consecutive amino acid residues for EThcD-based experiments (**Figure 4E**).

Finally, for the 56 kDa glutamate dehydrogenase, both ETD and EThcD MS^2 returned sequence coverages between 19% and 21%, with better results from the 70+ precursor

(**Figure S11A** and **Figure 5A**). A similar trend was observed for the number of unique matched fragments, with fewer than 100 distinct product ions identified in ETD MS^2 experiments and up to 123 for EThcD MS^2 (**Figure S11B** and **Figure 5B**). In the majority of cases, applying PTCR starting from a single wide isolation window of ETD or EThcD products did not prove beneficial in terms of overall sequence coverage: for ETD, the 1x1800 PTCR MS^3 experiments outperformed the MS^2 counterparts only starting from the 60+ precursor (that with the lowest charge); even in this case, the sequence coverage reached ~20%, not improving over the MS^2 results obtained from the 70+ charge state precursor (**Figure S11A**). Similarly, for EThcD, the 1x1800 PTCR MS^3 experiment that demonstrated the highest increase in sequence coverage was the one based on the 60+ precursor, which reached 28% sequence coverage (**Figure 5A**). A more substantial improvement in sequence coverage was obtained by applying the 6x250 PTCR MS^3 strategy, which outperformed both the MS^2 and the 1x1800 PTCR MS^3 experiments also in terms of number of identified fragments. Using the PTCR MS^3 strategy based on multiple isolation windows, ETD returned nearly 30% sequence coverage and almost 140 unique identified fragments, while these values increased to 36% and over 220, respectively, using EThcD. Partially paralleling the observations made for enolase, also for glutamate dehydrogenase the 1x1800 PTCR MS^3 strategy led to the identification of the largest product ions, but the highest median mass of fragments was obtained through the more complex 6x250 PTCR MS^3 data acquisition strategy (**Figure S11C** and **Figure 5C**). Likely due to the high charge states of the selected precursors, we observed that in ETD and EThcD MS^2 spectra of glutamate dehydrogenase most product ions were concentrated in a relatively limited spectral region of approximately 800-1000 m/z units (**Figure S12**). In light of this, we modified our 6x250 strategy by adapting both the width and center of the six isolation windows, to split the densely populated m/z window

spanning approximately from 800 to 1600 *m/z* into smaller batches and covering the remaining portions of the spectrum (down to *m/z* 200 and up to *m/z* 2000) using windows larger than the standard 270 *m/z* units (**Table S2**). This "alternate" 6x250 strategy proved beneficial for sequence coverage (which reached up to 32% for ETD and 39% for EThcD), number of identified fragments and even to retrieve some of the large fragments that, while identified by the simpler 1x1800 PTCR MS^3 experiments, were missed by the standard 6x250 PTCR MS^3 data acquisition. Importantly, while unsequenced regions of 30-40 consecutive amino acid residues remain even when applying the "alternate" 6x250 strategy, in general the characterization of the central portion of glutamate dehydrogenase was improved using PTCR, with both isolated matched cleavages and also 3-to-7 residue long "sequence tags" present between amino acids 150 and 350.

Regardless of the protein mass, in EThcD experiments *b*- and *y*-type ions generated via collisional activation of ETD products contributed to extend protein sequencing: these ions account for 10, 9, 8 and 13 unique cleavages not identified by *c*-/*z*-type ions in MS^2 experiments for carbonic anhydrase, aldolase, enolase and glutamate dehydrogenase, respectively. These numbers increase to 18, 16, 25 and 52 considering the 6x250 PTCR MS^3 experiments (see panels **E** of **Figures 2-5**). This observation corroborates the notion of complementarity between radical-driven ion activation methods and vibrational energy threshold ion activation techniques such as collision-induced dissociation and higher-energy collisional dissociation (HCD), which had been explored and demonstrated by multiple studies, even using the same standard proteins chosen for the present work.[31, 52]

Given the popularity of HCD in top-down proteomics, we also tested this fragmentation method and compared HCD MS^2 results with HCD MS^2 - 1x1800 PTCR MS^3 data acquisition. For each of the 12 total protein precursor ions investigated (three different charge states for each protein), PTCR allowed the identification of additional fragments and increased the matched fragments' median mass, not only leading to higher sequence coverages than the corresponding MS^2 experiments but also providing better characterization of the central portions of the proteins' sequences (**Figure S13-S16**). Similar to ETD and EThcD, HCD was capable of returning many complementary ion pairs, even for glutamate dehydrogenase, when fragmentation was followed by product ions' charge reduction. The application of PTCR brought HCD results almost on par with ETD and EThcD MS^2 ones: for example, HCD MS^2 - 1x1800 PTCR MS^3 returned more than 40% sequence coverage for the 50+ precursor of aldolase, in line with the corresponding electron-based fragmentation outcomes. As a results of PTCR efficacy in increasing the quality of HCD spectra, the combination of a single HCD MS^2 - 1x1800 PTCR MS^3 experiment with one EThcD MS^2 - 1x1800 PTCR MS^3 experiment elevates the sequence coverage for 46 kDa enolase up to 77%, largely outperforming the results obtained by EThcD MS^2 – PTCR MS^3 alone (**Figure 6A**). When the product ions of the same HCD MS^2 - 1x1800 PTCR MS^3 experiment are added to those derived from the EThcD MS^2 – 6x250 PTCR MS^3 experiments, the coverage is further improved to 80% (**Figure 6B**). The combination of HCD and EThcD charge-reduced fragments slightly increased also the coverage obtained for glutamate dehydrogenase: the sum of one HCD and one EThcD 1x1800 PTCR MS^3 run led up to 35% coverage (not far from the results of the alternate 6x250 PTCR MS^3 strategy), while summing HCD charge-reduced fragments to those obtained through the alternate 6x250 PTCR MS^3 strategy led to 44% sequence coverage, the highest value we registered for this 56 kDa protein (**Figure S17**).

Finally, until now we focused on results achievable via ETD, EThcD and HCD alone or in combination with PTCR, but we did not provide details about the optimization of the fragmentation conditions. Both tested ion-ion reactions (i.e., ETD and PTCR) were performed under conditions ensuring a pseudo-first order kinetics (i.e., large excess of the reagents, set to 1.5e6 charges for fluoranthene anions for all experiments and 2e6 charges for PFPP anions for MS^2 and 1x1800 PTCR MS3 while 1e6 charges of PFPP were used for 6-window PTCR MS^3 experiments). Keeping the total number of precursor charges fixed, we varied the reaction durations. Interestingly, the results shown in **Figure 7** demonstrates that longer ETD durations generally led to improved sequencing of the analyzed proteins: 5 ms was typically the best duration, with the exception of aldolase (where 3 and 5 ms returned very similar results, with a slight advantage for the former value) and glutamate dehydrogenase, where extending the activation to 7 ms helped identifying more product ions; it is possible this trend could continue to longer ETD activations. Typically, increasing ETD reaction duration favors the formation of multiple generations of product ions, resulting from larger and therefore higher charge state product ions (ETD reaction kinetics is proportional to z^2) undergoing further ETD reactions. This produces a plethora of low abundance internal fragments and a bias toward relatively abundant shorter C- and N-terminal sequence ions. Particularly in the case of large proteins, we hypothesize that forming second and greater generation fragments during MS^2 experiments can be beneficial for obtaining a higher sequence coverage as smaller product ions also have more variance in their degree of protonation relative to their masses and thus are distributed over a larger m/z range thus resulting in reduced overlapping of isotopic envelopes in the m/z domain. Further, detection of lower mass product ions is more sensitive in the Orbitrap analyzer at m/z resolutions appropriate for TDMS. Thus, independent of the issue of overlapping isotopic envelopes

due of spectral density, the detection of *m/z* peak isotopic clusters of lower mass fragment ions will likely be more sensitive (i.e., with improved S/N) than for much larger mass first-generation product ions. These hypotheses are supported by the analysis of the violin plots in **Figure S18**, showing that the median mass of matched product ions typically decreases, or at least remains stable, as the ETD reaction duration increases. Distributing product ions across a wider portion of the *m/z* space by reducing their size and charge state is conceptually similar to what achieved by subjecting product ions to PTCR. This strategy was recently applied with success to improve the sequencing of an intact antibody characterized by ETD and AI-ETD MS^2.[53] However, the best results obtained in PTCR MS^3 experiments were based on shorter ETD durations (**Figures S19-S22**), likely due to the fact that larger, first-generation product ions where maintained intact and could be detected once spectral congestion was reduced via deprotonation. Regarding the PTCR duration, for the 1x1800 PTCR MS^3 experiments we tested values of 20, 30 and 50 ms. Example spectra for different PTCR durations are shown in **Figure S23**. Generally, 20 ms PTCR provided the best results, followed by 30 ms. While 50 ms PTCR distributed fragments up to 7000-8000 *m/z*, excessive charge reduction resulted in the loss of several product ions (which is visible visually by comparing the 30 ms and 50 ms spectra in **Figure S23**) and thus in a decrease in sequence coverage.

Conclusions.

While the top-down approach for targeted and large-scale analysis of intact proteoforms is becoming more popular and the required technology accessible to many laboratories,[54] the effective restrictions of TDMS analysis to proteins <30 kDa represents a clear limitation. Even by applying well-tested sample preparation and data acquisition

protocols,[55] the gas-phase sequencing of large proteoforms remains an inherently complicated process. While preliminary results have demonstrated the potential of proton transfer reactions combined with parallel ion parking for TDMS experiments using a customized 21 T FT-ICR instrument at the National High Magnetic Field Laboratory,[56] in this study we demonstrated the advantages offered by a commercial high-resolution FTMS platform which natively incorporates PTCR capabilities along with an extended m/z range and efficient transmission of ions from the reaction cell (i.e., the LTQ) to the Orbitrap. Importantly, the above described EThcD MS^2 - PTCR MS^3 experiments returned higher sequencing than previous reports based on AI-ETD MS^2 (for carbonic anhydrase, aldolase and enolase)[31] or on 193 nm UVPD followed by proton transfer reaction MS^3 (for all four proteins investigated herein).[45] Admittedly, PTCR facilitates product ion identification, but it does not enhance ion dissociation. Therefore, we anticipate that implementing AI-ETD (possibly in combination product ion parking)[42] as well as UVPD on a PTCR-enabled Orbitrap Eclipse would enable further improvements in large protein (> 30 kDa) sequence coverage relative to the results reported in this study. Nonetheless, independent of the possibilities for further future improvements, we believe this work can establishe a blueprint for facilitating the thorough sequence analysis of any protein up to 60 kDa without the need of customized instrumentation.

Acknowledgements.

This work was supported by startup funds of the University of Oklahoma to L.F.

Conflict of interest.

C.M., J.E.P.S. and R.H. are employees of Thermo Scientific. K.R.D. is an employee of Proteinaceous, which commercializes software for the analysis of top-down mass spectrometry data.

Supporting Information.

Details on 6x250 PTCR MS^3 experiments, parameters for data analysis, summary of conditions tested for carbonic anhydrase, summary of conditions tested for aldolase, summary of conditions tested for enolase, summary of conditions tested for glutamate dehydrogenase, Venn diagrams of manual vs automatic spectral validation, ETD MS^2 spectrum of 42+ precursor charge state of aldolase, ETD MS^2 - PTCR MS^3 spectrum of the 42+ precursor charge state of aldolase, comparison of ETD MS^2 and ETD MS^2 - PTCR MS^3 experiments on carbonic anhydrase, comparison of ETD MS^2 and ETD MS^2 - PTCR MS^3 experiments on aldolase, comparison of ETD MS^2 and ETD MS^2 - PTCR MS^3 experiments on carbonic enolase, comparison of ETD MS^2 and ETD MS^2 - PTCR MS^3 experiments on carbonic gluatamate dehydrogenase, ETD and EThcD MS^2 spectra of glutamate dehydrogenase, comparison of HCD MS^2 and HCD MS^2 - PTCR MS^3 experiments on carbonic anhydrase, comparison of HCD MS^2 and HCD MS^2 - PTCR MS^3 experiments on aldolase, comparison of HCD MS^2 and HCD MS^2 - PTCR MS^3 experiments on enolase, comparison of HCD MS^2 and HCD MS^2 - PTCR MS^3 experiments on glutamate dehydrogenase, fragmentation maps of glutamate dehydrogenase combining HCD and EThcD PTCR MS^3 data, mass distribution of identified unique fragments in ETD experiments, sequence coverage vs PTCR duration for carbonic anhydrase, sequence coverage vs PTCR duration for aldolase, sequence coverage vs PTCR duration for carbonic enolase, sequence coverage vs PTCR duration for glutamate

dehydrogenase, EThcD MS^2 - PTCR MS^3 experiments with different PTCR durations.**Figure legends.**

Figure 1. Schematic representation of applied data acquisition schemes. In a standard MS^2 experiment (spectrum on the left) product ions generated in the LTQ or HCD cell are then transferred to the Orbitrap mass analyzer for high resolution detection. Alternatively, product ions can be isolated using a single, 1800 *m/z*-wide isolation window and subjected to PTCR prior to their detection in the Orbitrap ("1x1800" PTCR MS^3 experiment, spectrum on the right). Finally, sub-populations of product ions can be consecutively isolated via narrower isolation windows and subjected one by one to PTCR ("6x250" PTCR MS^3 experiment, bottom spectra).

Figure 2. Comparison of EThcD MS^2 and EThcD MS^2 - PTCR MS^3 experiments on carbonic anhydrase. (A) Sequence coverage for precursor ions 30+, 35+ and 40+. Error bars represent the standard deviation and experiments are color-coded. (B) Number of identified unique product ions for the same precursors. (C) Violin plots of the mass distributions of identified product ions (the thicker line represents the median, the dashed lines the first and third quartile). (D) EThcD MS^2 fragmentation map (from a single run). Red bars represent *c*-/*z*-type ions, blue bars *b*-/*y*-type ions. (E) EThcD MS^2 – 6x250 PTCR MS3 fragmentation map (from a single run).

Figure 3. Comparison of EThcD MS^2 and EThcD MS^2 - PTCR MS^3 experiments on aldolase. (A) Sequence coverage for precursor ions 42+, 47+ and 52+. (B) Number of identified unique product ions for the same precursors. (C) Violin plots of the mass distributions of identified product ions. (D) EThcD MS^2 fragmentation map (from a single run). (E) EThcD MS^2 – 6x250 PTCR MS^3 fragmentation map (from a single run).

Figure 4. Comparison of EThcD MS^2 and EThcD MS^2 - PTCR MS^3 experiments on enolase. (A) Sequence coverage for precursor ions 50+, 55+ and 60+. (B) Number of identified unique product ions for the same precursors. (C) Violin plots of the mass distributions of identified product ions. (D) EThcD MS^2 fragmentation map (from a single run). (E) EThcD MS^2 – 6x250 PTCR MS^3 fragmentation map (from a single run).

Figure 5. Comparison of EThcD MS^2 and EThcD MS^2 - PTCR MS^3 experiments on glutamate dehydrogenase. (A) Sequence coverage for precursor ions 60+, 65+ and 70+. (B) Number of identified unique product ions for the same precursors. (C) Violin plots of the mass distributions of identified product ions. (D) EThcD MS^2 fragmentation map (from a single run). (E) EThcD MS^2 – 6x250 PTCR MS^3 fragmentation map (from a single run).

Figure 6. Fragmentation maps of enolase combining a single HCD MS^2 – 1x1800 PTCR MS^3 experiment with different EThcD MS^2 – PTCR MS^3 experiments. (A) Fragment map based on fragments produced by a single 1x1800 PTCR MS^3 experiment. (B) Fragment map based on fragments produced by a single 6x250 PTCR MS^3 experiment.

Figure 7. Sequence coverage achieved via ETD MS^2 of the four proteins as a function of ETD duration. (A) Carbonic anhydrase. (B) Aldolase. (C) Enolase. (D) Glutamate dehydrogenase. Experiments on different precursor charge states are color-coded.

Figure 1

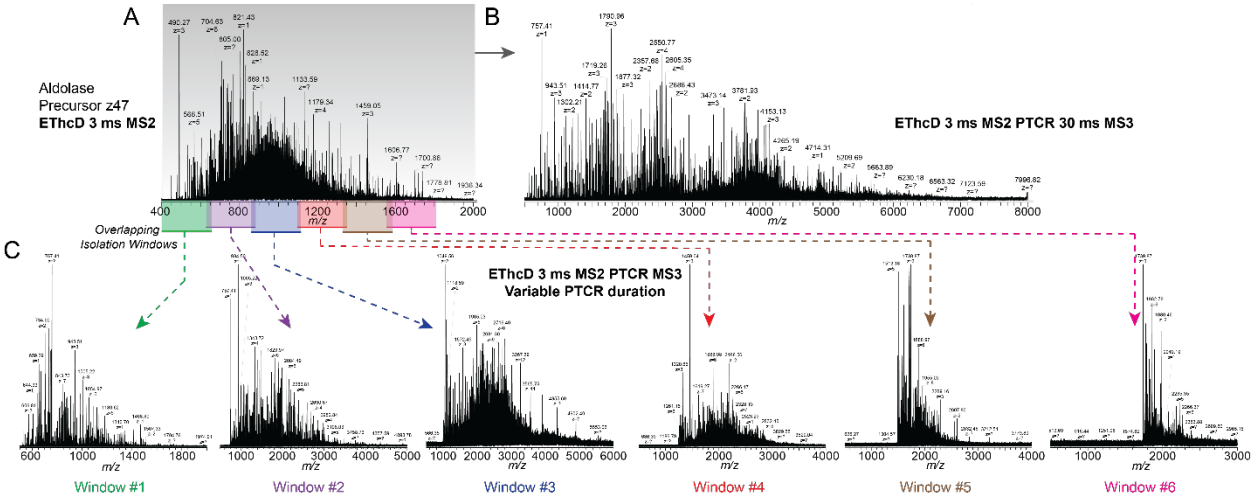
A
Aldolase
Precursor z47
EThcD 3 ms MS2
B
EThcD 3 ms MS2 PTCR 30 ms MS3
Overlapping
Isolation Windows
C
EThcD 3 ms MS2 PTCR MS3
Variable PTCR duration
m/z
Window #1
Window #2
Window #3
Window #4
Window #5
Window #6

Figure 2

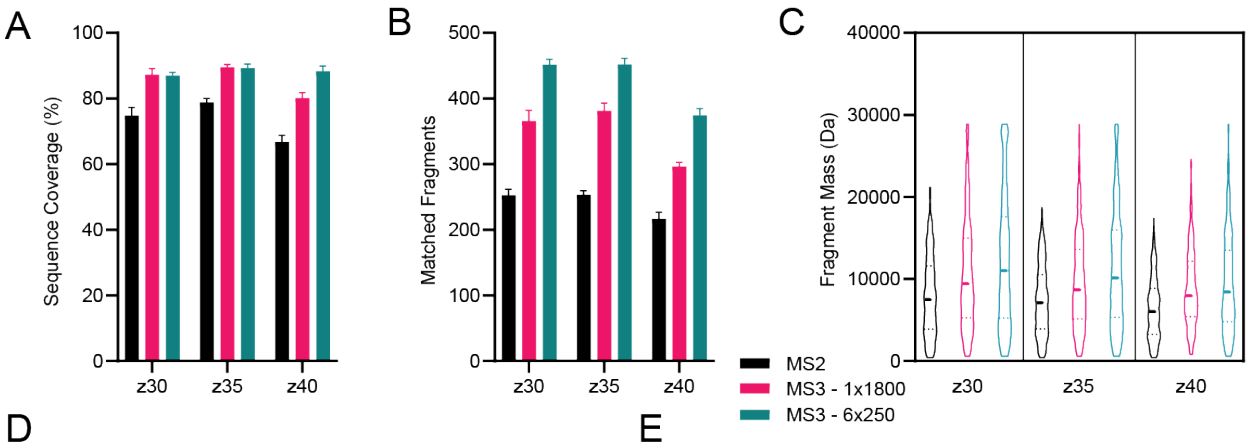
A
Sequence Coverage (%)
100
80
60
40
20
0
z30
z35
z40
B
Matched Fragments
500
400
300
200
100
0
z30
z35
z40
C
Fragment Mass (Da)
40000
30000
20000
10000
0
z30
z35
z40
MS2
MS3 - 1x1800
MS3 - 6x250

D

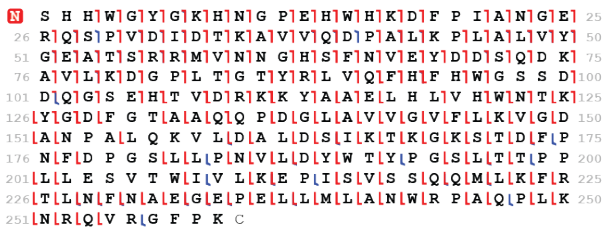
N S H H W G Y G K H N G P E H W H K D F P I A N G E 25
26 R Q S P V D I D T K A V V Q D P A L K P L A L V Y 50
51 G E A T S R R M V N N G H S F N V E Y D D S Q D K 75
76 A V L K D G P L T G T Y R L V Q F H F H W G S S D 100
101 D Q G S E H T V D R K K Y A A E L H L V H W N T K 125
126 Y G D F G T A A Q Q P D G L A V V G V F L K V G D 150
151 A N P A L Q K V L D A L D S I K T K G K S T D F P 175
176 N F D P G S L L P N V L D Y W T Y P G S L T T P P 200
201 L L E S V T W I V L K E P I S V S S Q Q M L K F R 225
226 T L N F N A E G E P E L L M L A N W R P A Q P L K 250
251 N R Q V R G F P K C

E

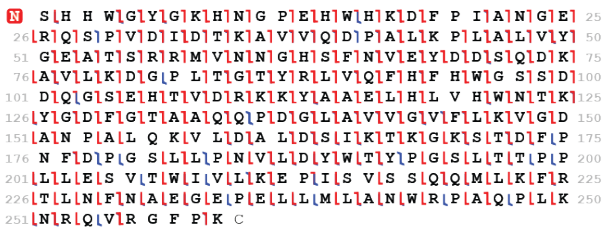
N S H H W G Y G K H N G P E H W H K D F P I A N G E 25
26 R Q S P V D I D T K A V V Q D P A L K P L A L V Y 50
51 G E A T S R R M V N N G H S F N V E Y D D S Q D K 75
76 A V L K D G P L T G T Y R L V Q F H F H W G S S D 100
101 D Q G S E H T V D R K K Y A A E L H L V H W N T K 125
126 Y G D F G T A A Q Q P D G L A V V G V F L K V G D 150
151 A N P A L Q K V L D A L D S I K T K G K S T D F P 175
176 N F D P G S L L P N V L D Y W T Y P G S L T T P P 200
201 L L E S V T W I V L K E P I S V S S Q Q M L K F R 225
226 T L N F N A E G E P E L L M L A N W R P A Q P L K 250
251 N R Q V R G F P K C

Figure 3.

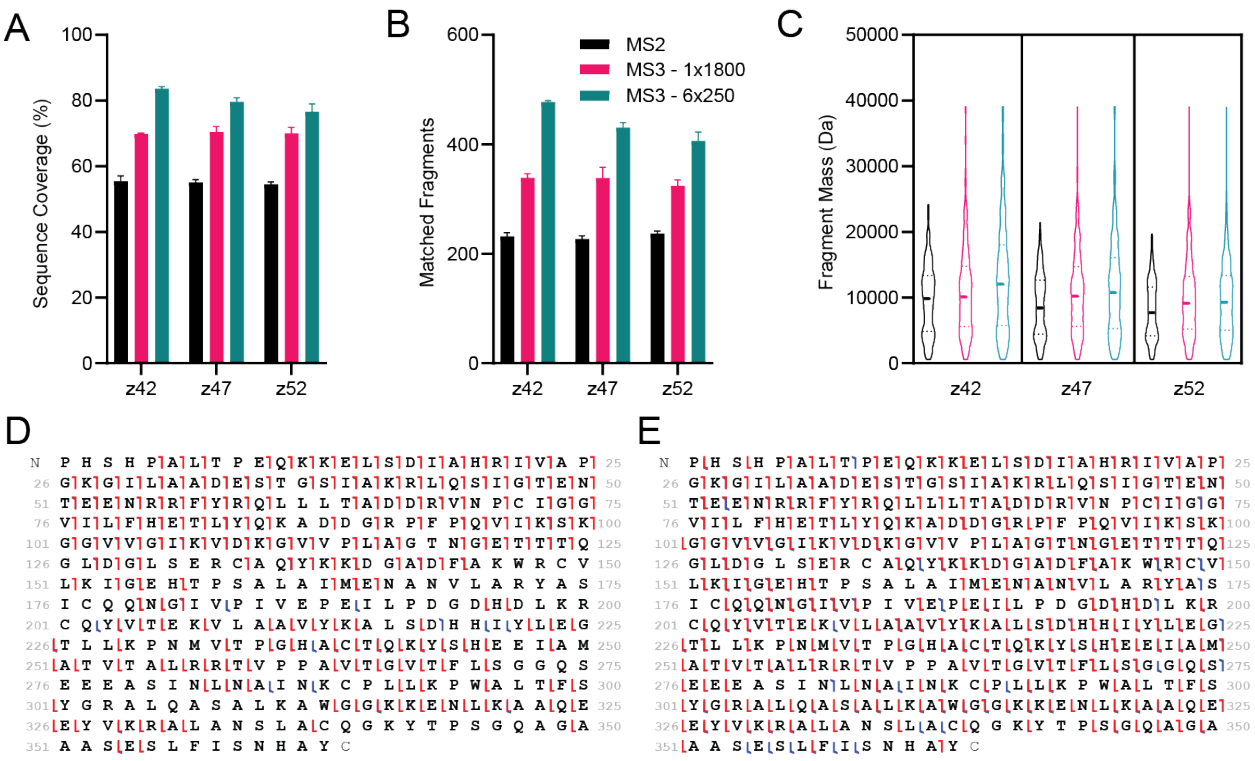
A
Sequence Coverage (%)
100
80
60
40
20
0
z42
z47
z52
B
Matched Fragments
600
400
200
0
MS2
MS3 - 1x1800
MS3 - 6x250
C
Fragment Mass (Da)
50000
40000
30000
20000
10000
0
D
E

Figure 4

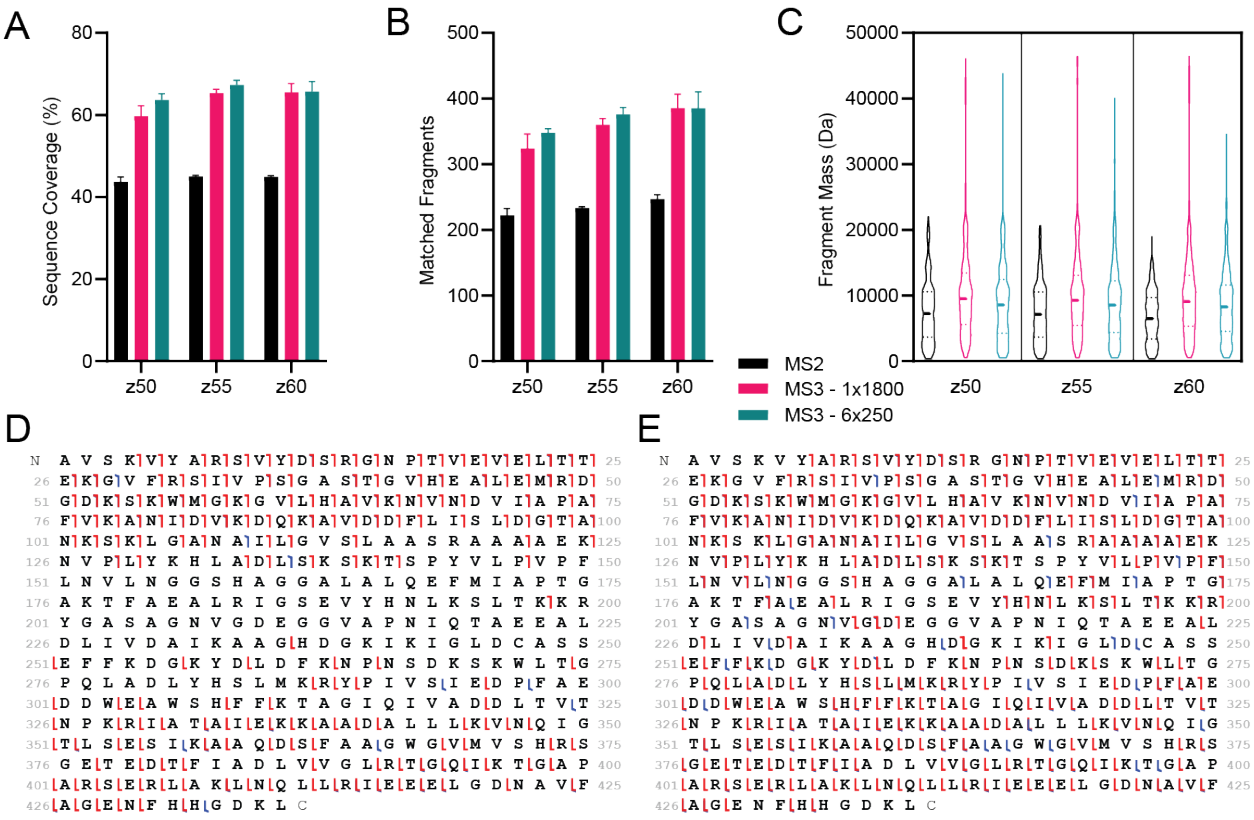
A
Sequence Coverage (%)
80
60
40
20
0
z50
z55
z60
B
Matched Fragments
500
400
300
200
100
0
z50
z55
z60
C
Fragment Mass (Da)
50000
40000
30000
20000
10000
0
z50
z55
z60
MS2
MS3 - 1x1800
MS3 - 6x250
D
E

Figure 5

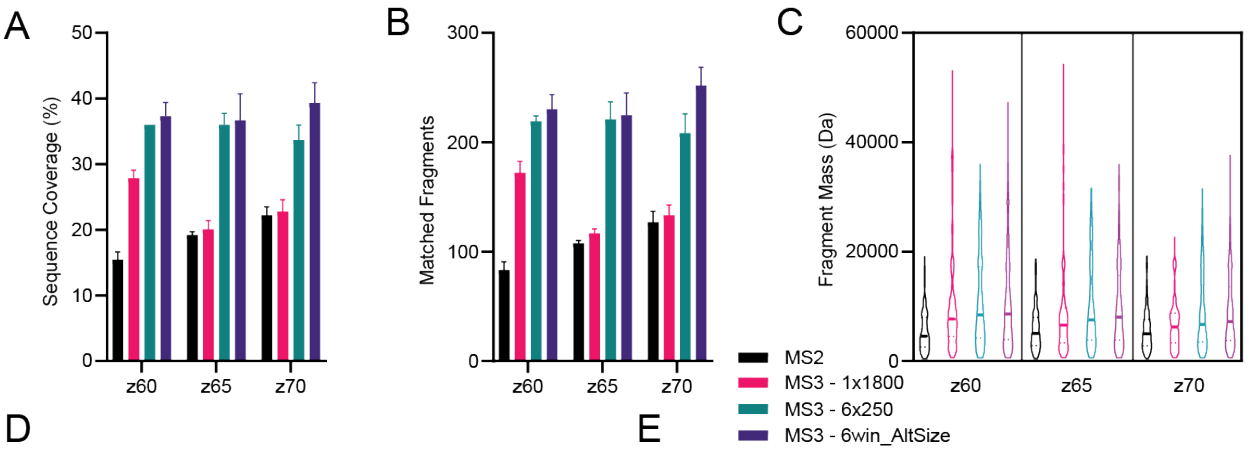
A
Sequence Coverage (%)
50
40
30
20
10
0
z60
z65
z70
B
Matched Fragments
300
200
100
0
z60
z65
z70
C
Fragment Mass (Da)
60000
40000
20000
0
z60
z65
z70
MS2
MS3 - 1x1800
MS3 - 6x250
MS3 - 6win_AltSize

D

E

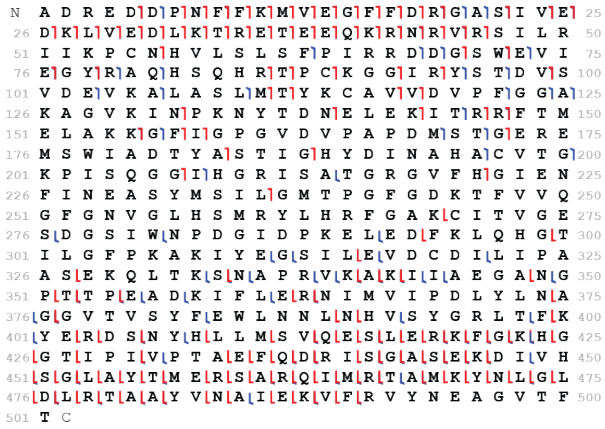

Figure 6

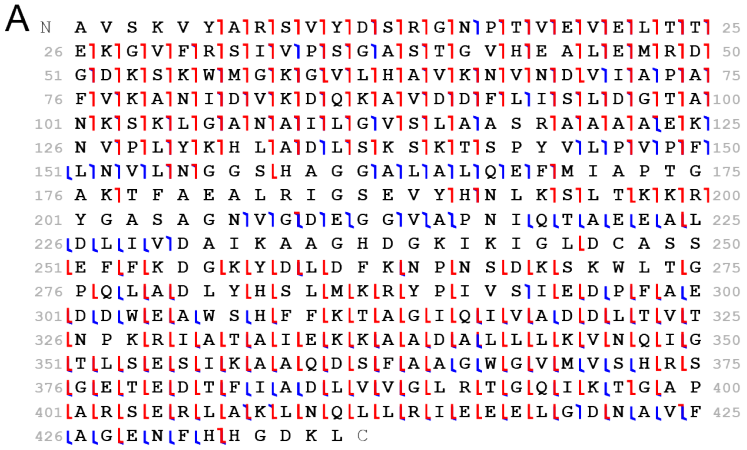
A
N A V S K V Y A R S V Y D S R G N P T V E V E L T T 25
26 E K G V F R S I V P S G A S T G V H E A L E M R D 50
51 G D K S K W M G K G V L H A V K N V N D V I A P A 75
76 F V K A N I D V K D Q K A V D D F L I S L D G T A 100
101 N K S K L G A N A I L G V S L A A S R A A A A E K 125
126 N V P L Y K H L A D L S K S K T S P Y V L P V P F 150
151 L N V L N G G S H A G G A L A L Q E F M I A P T G 175
176 A K T F A E A L R I G S E V Y H N L K S L T K K R 200
201 Y G A S A G N V G D E G G V A P N I Q L T A E E A L 225
226 D L L I V D A I K A A G H D G K I K I G L D C A S S 250
251 E F F K D G K Y D L L D F K N P N S D K S K W L T G 275
276 P Q L L A D L Y H S L M K R Y P I V S I E D P F A E 300
301 D D W E A W S H F F K T A G I Q I V A D D L T V T 325
326 N P K R I A T A I E K K A A D A L L L K V N Q I G 350
351 T L S E S I K A A Q D S F A A G W G V M V S H R S 375
376 G E T E D T F I A D L V V G L R T G Q I K T G A P 400
401 A R S E R L A K L N Q L L R I E E E L G D N A V F 425
426 A G E N F H H G D K L C
HCD MS2 - 1x1800 PTCR MS3 with EThcD MS2 - 1x1800 PTCR MS3
Sequence coverage: 77%
B
N A V S K V Y A R S V Y D S R G N P T V E V E L T T 25
26 E K G V F R S I V P S G A S T G V H E A L E M R D 50
51 G D K S K W M G K G V L H A V K N V N D V I A P A 75
76 F V K A N I D V K D Q K A V D D F L I S L D G T A 100
101 N K S K L G A N A I L G V S L A A S R A A A A E K 125
126 N V P L Y K H L A D L S K S K T S P Y V L P V P F 150
151 L N V L N G G S H A G G A L A L Q E F M I A P T G 175
176 A K T F A E A L R I G S E V Y H N L K S L T K K R 200
201 Y G A S A G N V G D E G G V A P N I Q L T A E E A L 225
226 D L L I V D A I K A A G H D G K I K I G L D C A S S 250
251 E F F K D G K Y D L L D F K N P N S D K S K W L T G 275
276 P Q L L A D L Y H S L M K R Y P I V S I E D P F A E 300
301 D D W E A W S H F F K T A G I Q I V A D D L T V T 325
326 N P K R I A T A I E K K A A D A L L L K V N Q I G 350
351 T L S E S I K A A Q D S F A A G W G V M V S H R S 375
376 G E T E D T F I A D L V V G L R T G Q I K T G A P 400
401 A R S E R L A K L N Q L L R I E E E L G D N A V F 425
426 A G E N F H H G D K L C
HCD MS2 - 1x1800 PTCR MS3 with EThcD MS2 - 6x250 PTCR MS3
Sequence coverage: 80%

Figure 7

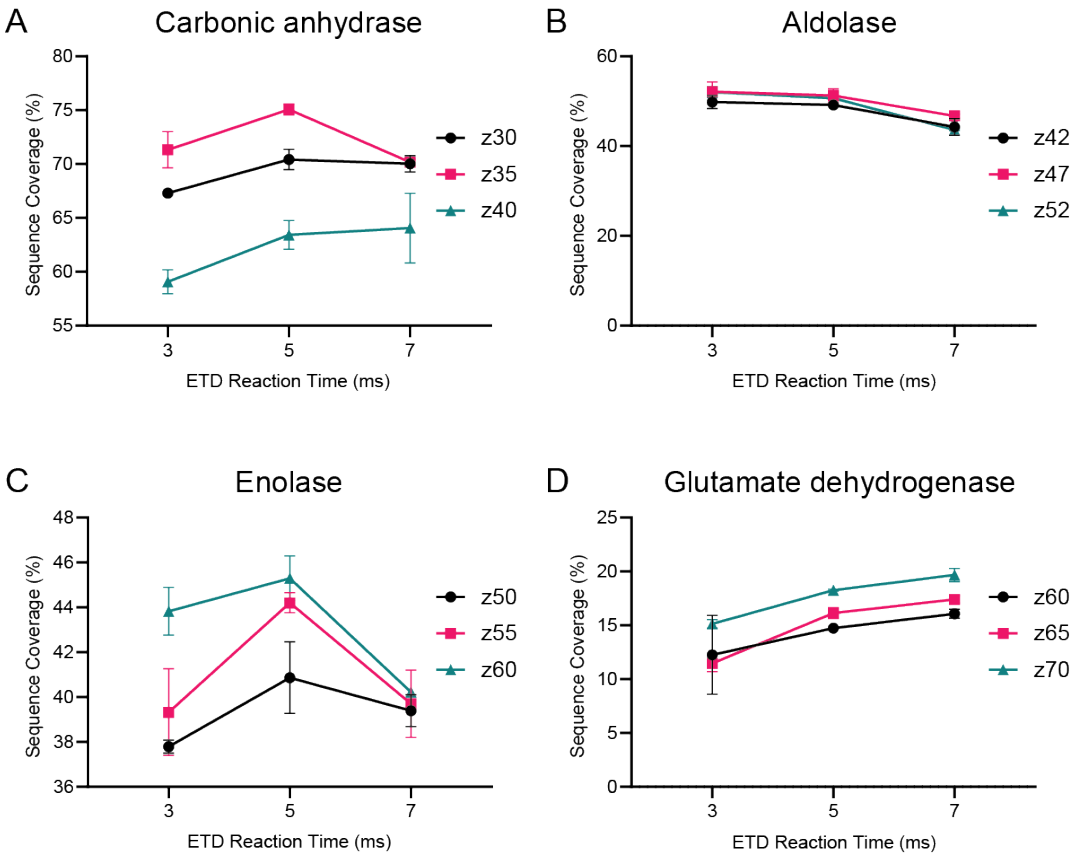
A
Carbonic anhydrase
Sequence Coverage (%)
80
75
70
65
60
55
3
5
7
ETD Reaction Time (ms)
z30
z35
z40
B
Aldolase
Sequence Coverage (%)
60
40
20
0
3
5
7
ETD Reaction Time (ms)
z42
z47
z52
C
Enolase
Sequence Coverage (%)
48
46
44
42
40
38
36
3
5
7
ETD Reaction Time (ms)
z50
z55
z60
D
Glutamate dehydrogenase
Sequence Coverage (%)
25
20
15
10
5
0
3
5
7
ETD Reaction Time (ms)
z60
z65
z70

References.

1. Toby, T. K.; Fornelli, L.; Kelleher, N. L., Progress in Top-Down Proteomics and the Analysis of Proteoforms. *Annu Rev Anal Chem (Palo Alto Calif)* **2016,** *9* (1), 499-519.
2. Smith, L. M.; Kelleher, N. L.; Consortium for Top Down, P., Proteoform: a single term describing protein complexity. *Nat Methods* **2013,** *10* (3), 186-7.
3. Zheng, Y.; Fornelli, L.; Compton, P. D.; Sharma, S.; Canterbury, J.; Mullen, C.; Zabrouskov, V.; Fellers, R. T.; Thomas, P. M.; Licht, J. D.; Senko, M. W.; Kelleher, N. L., Unabridged Analysis of Human Histone H3 by Differential Top-Down Mass Spectrometry Reveals Hypermethylated Proteoforms from MMSET/NSD2 Overexpression. *Mol Cell Proteomics* **2016,** *15* (3), 776-90.
4. Greer, S. M.; Brodbelt, J. S., Top-Down Characterization of Heavily Modified Histones Using 193 nm Ultraviolet Photodissociation Mass Spectrometry. *J Proteome Res* **2018,** *17* (3), 1138-1145.
5. Brodbelt, J. S., Ion Activation Methods for Peptides and Proteins. *Anal Chem* **2016,** *88* (1), 30-51.
6. Zhurov, K. O.; Fornelli, L.; Wodrich, M. D.; Laskay, U. A.; Tsybin, Y. O., Principles of electron capture and transfer dissociation mass spectrometry applied to peptide and protein structure analysis. *Chem Soc Rev* **2013,** *42* (12), 5014-30.
7. Brodbelt, J. S.; Morrison, L. J.; Santos, I., Ultraviolet Photodissociation Mass Spectrometry for Analysis of Biological Molecules. *Chem Rev* **2020,** *120* (7), 3328-3380.
8. Zubarev, R. A.; Horn, D. M.; Fridriksson, E. K.; Kelleher, N. L.; Kruger, N. A.; Lewis, M. A.; Carpenter, B. K.; McLafferty, F. W., Electron capture dissociation for structural characterization of multiply charged protein cations. *Anal Chem* **2000,** *72* (3), 563-73.
9. Syka, J. E.; Coon, J. J.; Schroeder, M. J.; Shabanowitz, J.; Hunt, D. F., Peptide and protein sequence analysis by electron transfer dissociation mass spectrometry. *Proc Natl Acad Sci U S A* **2004,** *101* (26), 9528-33.
10. Tsybin, Y. O.; Quinn, J. P.; Tsybin, O. Y.; Hendrickson, C. L.; Marshall, A. G., Electron capture dissociation implementation progress in Fourier transform ion cyclotron resonance mass spectrometry. *J Am Soc Mass Spectrom* **2008,** *19* (6), 762-71.
11. Ge, Y.; Rybakova, I. N.; Xu, Q.; Moss, R. L., Top-down high-resolution mass spectrometry of cardiac myosin binding protein C revealed that truncation alters protein phosphorylation state. *Proc Natl Acad Sci U S A* **2009,** *106* (31), 12658-63.
12. Mao, Y.; Valeja, S. G.; Rouse, J. C.; Hendrickson, C. L.; Marshall, A. G., Top-down structural analysis of an intact monoclonal antibody by electron capture dissociation-Fourier transform ion cyclotron resonance-mass spectrometry. *Anal Chem* **2013,** *85* (9), 4239-46.
13. Williams, J. P.; Morrison, L. J.; Brown, J. M.; Beckman, J. S.; Voinov, V. G.; Lermyte, F., Top-Down Characterization of Denatured Proteins and Native Protein Complexes Using Electron Capture Dissociation Implemented within a Modified Ion Mobility-Mass Spectrometer. *Anal Chem* **2020,** *92* (5), 3674-3681.
14. Shaw, J. B.; Malhan, N.; Vasil'ev, Y. V.; Lopez, N. I.; Makarov, A.; Beckman, J. S.; Voinov, V. G., Sequencing Grade Tandem Mass Spectrometry for Top-Down Proteomics Using Hybrid Electron Capture Dissociation Methods in a Benchtop Orbitrap Mass Spectrometer. *Anal Chem* **2018,** *90* (18), 10819-10827.
15. McAlister, G. C.; Berggren, W. T.; Griep-Raming, J.; Horning, S.; Makarov, A.; Phanstiel, D.; Stafford, G.; Swaney, D. L.; Syka, J. E.; Zabrouskov, V.; Coon, J. J., A

proteomics grade electron transfer dissociation-enabled hybrid linear ion trap-orbitrap mass spectrometer. *J Proteome Res* **2008,** *7* (8), 3127-36.
16. Coelho Graca, D.; Lescuyer, P.; Clerici, L.; Tsybin, Y. O.; Hartmer, R.; Meyer, M.; Samii, K.; Hochstrasser, D. F.; Scherl, A., Electron transfer dissociation mass spectrometry of hemoglobin on clinical samples. *J Am Soc Mass Spectrom* **2012,** *23* (10), 1750-6.
17. Fornelli, L.; Parra, J.; Hartmer, R.; Stoermer, C.; Lubeck, M.; Tsybin, Y. O., Top-down analysis of 30-80 kDa proteins by electron transfer dissociation time-of-flight mass spectrometry. *Anal Bioanal Chem* **2013,** *405* (26), 8505-14.
18. Tsybin, Y. O.; Fornelli, L.; Stoermer, C.; Luebeck, M.; Parra, J.; Nallet, S.; Wurm, F. M.; Hartmer, R., Structural analysis of intact monoclonal antibodies by electron transfer dissociation mass spectrometry. *Anal Chem* **2011,** *83* (23), 8919-27.
19. Fornelli, L.; Damoc, E.; Thomas, P. M.; Kelleher, N. L.; Aizikov, K.; Denisov, E.; Makarov, A.; Tsybin, Y. O., Analysis of intact monoclonal antibody IgG1 by electron transfer dissociation Orbitrap FTMS. *Mol Cell Proteomics* **2012,** *11* (12), 1758-67.
20. Fornelli, L.; Srzentic, K.; Huguet, R.; Mullen, C.; Sharma, S.; Zabrouskov, V.; Fellers, R. T.; Durbin, K. R.; Compton, P. D.; Kelleher, N. L., Accurate Sequence Analysis of a Monoclonal Antibody by Top-Down and Middle-Down Orbitrap Mass Spectrometry Applying Multiple Ion Activation Techniques. *Anal Chem* **2018,** *90* (14), 8421-8429.
21. Fornelli, L.; Ayoub, D.; Aizikov, K.; Liu, X.; Damoc, E.; Pevzner, P. A.; Makarov, A.; Beck, A.; Tsybin, Y. O., Top-down analysis of immunoglobulin G isotypes 1 and 2 with electron transfer dissociation on a high-field Orbitrap mass spectrometer. *J Proteomics* **2017,** *159*, 67-76.
22. Horn, D. M.; Ge, Y.; McLafferty, F. W., Activated ion electron capture dissociation for mass spectral sequencing of larger (42 kDa) proteins. *Anal Chem* **2000,** *72* (20), 4778-84.
23. Riley, N. M.; Coon, J. J., The Role of Electron Transfer Dissociation in Modern Proteomics. *Anal Chem* **2018,** *90* (1), 40-64.
24. Fornelli, L.; Toby, T. K., Chapter 3 ECD/ETD for Sequencing of Peptides and Denatured Proteins. In *Advanced Fragmentation Methods in Biomolecular Mass Spectrometry: Probing Primary and Higher Order Structure with Electrons, Photons and Surfaces*, The Royal Society of Chemistry: 2021; pp 33-71.
25. Swaney, D. L.; McAlister, G. C.; Wirtala, M.; Schwartz, J. C.; Syka, J. E.; Coon, J. J., Supplemental activation method for high-efficiency electron-transfer dissociation of doubly protonated peptide precursors. *Anal Chem* **2007,** *79* (2), 477-85.
26. Olsen, J. V.; Macek, B.; Lange, O.; Makarov, A.; Horning, S.; Mann, M., Higher-energy C-trap dissociation for peptide modification analysis. *Nat Methods* **2007,** *4* (9), 709-12.
27. Brunner, A. M.; Lossl, P.; Liu, F.; Huguet, R.; Mullen, C.; Yamashita, M.; Zabrouskov, V.; Makarov, A.; Altelaar, A. F.; Heck, A. J., Benchmarking multiple fragmentation methods on an orbitrap fusion for top-down phospho-proteoform characterization. *Anal Chem* **2015,** *87* (8), 4152-8.
28. Riley, N. M.; Westphall, M. S.; Coon, J. J., Activated Ion-Electron Transfer Dissociation Enables Comprehensive Top-Down Protein Fragmentation. *J Proteome Res* **2017,** *16* (7), 2653-2659.
29. Riley, N. M.; Westphall, M. S.; Coon, J. J., Activated Ion Electron Transfer Dissociation for Improved Fragmentation of Intact Proteins. *Anal Chem* **2015,** *87* (14), 7109-16.
30. Riley, N. M.; Sikora, J. W.; Seckler, H. S.; Greer, J. B.; Fellers, R. T.; LeDuc, R. D.; Westphall, M. S.; Thomas, P. M.; Kelleher, N. L.; Coon, J. J., The Value of Activated

Ion Electron Transfer Dissociation for High-Throughput Top-Down Characterization of Intact Proteins. *Anal Chem* **2018,** *90* (14), 8553-8560.
31. Riley, N. M.; Westphall, M. S.; Coon, J. J., Sequencing Larger Intact Proteins (30-70 kDa) with Activated Ion Electron Transfer Dissociation. *J Am Soc Mass Spectrom* **2018,** *29* (1), 140-149.
32. Shaw, J. B.; Li, W.; Holden, D. D.; Zhang, Y.; Griep-Raming, J.; Fellers, R. T.; Early, B. P.; Thomas, P. M.; Kelleher, N. L.; Brodbelt, J. S., Complete protein characterization using top-down mass spectrometry and ultraviolet photodissociation. *J Am Chem Soc* **2013,** *135* (34), 12646-51.
33. Fornelli, L.; Srzentic, K.; Toby, T. K.; Doubleday, P. F.; Huguet, R.; Mullen, C.; Melani, R. D.; Dos Santos Seckler, H.; DeHart, C. J.; Weisbrod, C. R.; Durbin, K. R.; Greer, J. B.; Early, B. P.; Fellers, R. T.; Zabrouskov, V.; Thomas, P. M.; Compton, P. D.; Kelleher, N. L., Thorough Performance Evaluation of 213 nm Ultraviolet Photodissociation for Top-down Proteomics. *Mol Cell Proteomics* **2020,** *19* (2), 405-420.
34. Cleland, T. P.; DeHart, C. J.; Fellers, R. T.; VanNispen, A. J.; Greer, J. B.; LeDuc, R. D.; Parker, W. R.; Thomas, P. M.; Kelleher, N. L.; Brodbelt, J. S., High-Throughput Analysis of Intact Human Proteins Using UVPD and HCD on an Orbitrap Mass Spectrometer. *J Proteome Res* **2017,** *16* (5), 2072-2079.
35. Compton, P. D.; Zamdborg, L.; Thomas, P. M.; Kelleher, N. L., On the scalability and requirements of whole protein mass spectrometry. *Anal Chem* **2011,** *83* (17), 6868-74.
36. Fornelli, L.; Durbin, K. R.; Fellers, R. T.; Early, B. P.; Greer, J. B.; LeDuc, R. D.; Compton, P. D.; Kelleher, N. L., Advancing Top-down Analysis of the Human Proteome Using a Benchtop Quadrupole-Orbitrap Mass Spectrometer. *J Proteome Res* **2017,** *16* (2), 609-618.
37. Prentice, B. M.; Ryan, D. J.; Grove, K. J.; Cornett, D. S.; Caprioli, R. M.; Spraggins, J. M., Dynamic Range Expansion by Gas-Phase Ion Fractionation and Enrichment for Imaging Mass Spectrometry. *Anal Chem* **2020,** *92* (19), 13092-13100.
38. McLuckey, S. A.; Huang, T. Y., Ion/ion reactions: new chemistry for analytical MS. *Anal Chem* **2009,** *81* (21), 8669-76.
39. Prentice, B. M.; McLuckey, S. A., Gas-phase ion/ion reactions of peptides and proteins: acid/base, redox, and covalent chemistries. *Chem Commun (Camb)* **2013,** *49* (10), 947-65.
40. Stephenson, J. L.; McLuckey, S. A., Ion/Ion Reactions in the Gas Phase: Proton Transfer Reactions Involving Multiply-Charged Proteins. *Journal of the American Chemical Society* **1996,** *118* (31), 7390-7397.
41. Stephenson, J. L., Jr.; McLuckey, S. A., Simplification of product ion spectra derived from multiply charged parent ions via ion/ion chemistry. *Anal Chem* **1998,** *70* (17), 3533-44.
42. Ugrin, S. A.; English, A. M.; Syka, J. E. P.; Bai, D. L.; Anderson, L. C.; Shabanowitz, J.; Hunt, D. F., Ion-Ion Proton Transfer and Parallel Ion Parking for the Analysis of Mixtures of Intact Proteins on a Modified Orbitrap Mass Analyzer. *J Am Soc Mass Spectrom* **2019,** *30* (10), 2163-2173.
43. McLuckey, S. A., The emerging role of ion/ion reactions in biological mass spectrometry: considerations for reagent ion selection. *Eur J Mass Spectrom (Chichester)* **2010,** *16* (3), 429-36.
44. Anderson, L. C.; English, A. M.; Wang, W.; Bai, D. L.; Shabanowitz, J.; Hunt, D. F., Protein derivatization and sequential ion/ion reactions to enhance sequence coverage produced by electron transfer dissociation mass spectrometry. *Int J Mass Spectrom* **2015,** *377*, 617-624.

45. Sanders, J. D.; Mullen, C.; Watts, E.; Holden, D. D.; Syka, J. E. P.; Schwartz, J. C.; Brodbelt, J. S., Enhanced Sequence Coverage of Large Proteins by Combining Ultraviolet Photodissociation with Proton Transfer Reactions. *Anal Chem* **2020,** *92* (1), 1041-1049.
46. Holden, D. D.; McGee, W. M.; Brodbelt, J. S., Integration of Ultraviolet Photodissociation with Proton Transfer Reactions and Ion Parking for Analysis of Intact Proteins. *Anal Chem* **2016,** *88* (1), 1008-16.
47. Huguet, R.; Mullen, C.; Srzentic, K.; Greer, J. B.; Fellers, R. T.; Zabrouskov, V.; Syka, J. E. P.; Kelleher, N. L.; Fornelli, L., Proton Transfer Charge Reduction Enables High-Throughput Top-Down Analysis of Large Proteoforms. *Anal Chem* **2019,** *91* (24), 15732-15739.
48. Earley, L.; Anderson, L. C.; Bai, D. L.; Mullen, C.; Syka, J. E.; English, A. M.; Dunyach, J. J.; Stafford, G. C., Jr.; Shabanowitz, J.; Hunt, D. F.; Compton, P. D., Front-end electron transfer dissociation: a new ionization source. *Anal Chem* **2013,** *85* (17), 8385-90.
49. Fellers, R. T.; Greer, J. B.; Early, B. P.; Yu, X.; LeDuc, R. D.; Kelleher, N. L.; Thomas, P. M., ProSight Lite: graphical software to analyze top-down mass spectrometry data. *Proteomics* **2015,** *15* (7), 1235-8.
50. DeHart, C. J.; Fellers, R. T.; Fornelli, L.; Kelleher, N. L.; Thomas, P. M., Bioinformatics Analysis of Top-Down Mass Spectrometry Data with ProSight Lite. In *Protein Bioinformatics: From Protein Modifications and Networks to Proteomics*, Wu, C. H.; Arighi, C. N.; Ross, K. E., Eds. Springer New York: New York, NY, 2017; pp 381-394.
51. Shaw, J. B.; Robinson, E. W.; Pasa-Tolic, L., Vacuum Ultraviolet Photodissociation and Fourier Transform-Ion Cyclotron Resonance (FT-ICR) Mass Spectrometry: Revisited. *Anal Chem* **2016,** *88* (6), 3019-23.
52. Weisbrod, C. R.; Anderson, L. C.; Greer, J. B.; DeHart, C. J.; Hendrickson, C. L., Increased Single-Spectrum Top-Down Protein Sequence Coverage in Trapping Mass Spectrometers with Chimeric Ion Loading. *Anal Chem* **2020,** *92* (18), 12193-12200.
53. Lodge, J. M.; Schauer, K. L.; Brademan, D. R.; Riley, N. M.; Shishkova, E.; Westphall, M. S.; Coon, J. J., Top-Down Characterization of an Intact Monoclonal Antibody Using Activated Ion Electron Transfer Dissociation. *Anal Chem* **2020,** *92* (15), 10246-10251.
54. Smith, L. M.; Kelleher, N. L., Proteoforms as the next proteomics currency. *Science* **2018,** *359* (6380), 1106-1107.
55. Donnelly, D. P.; Rawlins, C. M.; DeHart, C. J.; Fornelli, L.; Schachner, L. F.; Lin, Z.; Lippens, J. L.; Aluri, K. C.; Sarin, R.; Chen, B.; Lantz, C.; Jung, W.; Johnson, K. R.; Koller, A.; Wolff, J. J.; Campuzano, I. D. G.; Auclair, J. R.; Ivanov, A. R.; Whitelegge, J. P.; Pasa-Tolic, L.; Chamot-Rooke, J.; Danis, P. O.; Smith, L. M.; Tsybin, Y. O.; Loo, J. A.; Ge, Y.; Kelleher, N. L.; Agar, J. N., Best practices and benchmarks for intact protein analysis for top-down mass spectrometry. *Nat Methods* **2019,** *16* (7), 587-594.
56. Weisbrod, C. R.; Anderson, L. C.; Shabanowitz, J.; Hunt, D. F.; Hendrickson, C. L., Proton Transfer Reactions and Parallel Ion Parking for Intact Protein Analysis on a 21 T FT-ICR Mass Spectrometer. *Proceedings of the 67th Annual Conference on Mass Spectrometry and Allied Topics* **2019**.